Biophysical Journal Volume 108 January 2015 203–210

Article

Modified Protein Expression in the Tectorial Membrane of the Cochlea Reveals Roles for the Striated Sheet Matrix

Gareth P. Jones,[1] Stephen J. Elliott,[2] Ian J. Russell,[1,*] and Andrei N. Lukashkin[1,*]

[1]School of Pharmacy and Biomolecular Sciences, University of Brighton, Brighton, United Kingdom; and [2]Institute of Sound and Vibration Research, University of Southampton, Southampton, United Kingdom

ABSTRACT The tectorial membrane (TM) of the mammalian cochlea is a complex extracellular matrix which, in response to acoustic stimulation, displaces the hair bundles of outer hair cells (OHCs), thereby initiating sensory transduction and amplification. Here, using TM segments from the basal, high-frequency region of the cochleae of genetically modified mice (including models of human hereditary deafness) with missing or modified TM proteins, we demonstrate that frequency-dependent stiffening is associated with the striated sheet matrix (SSM). Frequency-dependent stiffening largely disappeared in all three TM mutations studied where the SSM was absent either entirely or at least from the stiffest part of the TM overlying the OHCs. In all three TM mutations, dissipation of energy is decreased at low (<8 kHz) and increased at high (>8 kHz) stimulus frequencies. The SSM is composed of polypeptides carrying fixed charges, and electrostatic interaction between them may account for frequency-dependent stiffness changes in the material properties of the TM. Through comparison with previous in vivo measurements, it is proposed that implementation of frequency-dependent stiffening of the TM in the OHC attachment region facilitates interaction among tones, backward transmission of energy, and amplification in the cochlea.

INTRODUCTION

The detection of sound in the mammalian cochlea is mediated via the organ of Corti (OC), a remarkable integration of extracellular matrices, cytoskeletal architecture, and molecular machinery. Each element of the OC has specific electrical and mechanical properties to facilitate transmission of acoustic energy along the cochlea, decompose complex sounds into individual frequency components, and (through rapid mechanoelectrical-electromechanical processes) amplify mechanical movements and convert them into electrical signals across vast ranges of frequencies and levels (1). The stiffness of the basilar membrane (BM) of the OC increases from the apex of the cochlea to its base (2). This gradient of stiffness provides the mechanical basis for cochlear frequency tuning with low-frequency vibrations of the BM peaking near the apex of the cochlea and high frequencies peaking near the base (2). Miniscule amounts of energy transmitted by the BM vibrations cause shear displacements between the apical surface of the OC and another extracellular matrix, the tectorial membrane (TM), into which the tips of the stereocilia of the outer hair cells (OHCs) are imbedded (3). The resultant modulation of current flow through the OHC serves as a control signal for the cochlear amplifier (4,5), which amplifies and sharpens the BM vibrations at the frequency-specific place (6).

The TM is a viscoelastic structure (7) that decreases in both width and thickness from cochlea apex to base and has longitudinal anisotropy (8–12) paralleling that of the BM (6). Interaction between BM and TM traveling waves has been hypothesized to control the spatial extent and timing of OHC excitation, which affects both gain and frequency tuning in the cochlea (13–16). Timing of the TM and BM traveling waves determines the relative shear motion between the OC and the TM (17,18). In 2013, it was found that the mechanical properties of the TM varied with stimulus frequency (19), a property that has yet to be considered in cochlear models.

According to this new finding, energy transmission along the various structures in the cochlea, which are submerged in fluid, is optimized—thereby enhancing amplification of signals at the frequency-specific place (19). The structural/physicochemical basis for the frequency dependence of the TM's mechanical properties is, however, unknown. It is worth noting that the frequency-dependent mechanical properties of living cells (20–22), including the OHCs (23), have been well documented. This frequency dependence is associated with the structurally complex cytoskeleton. In this sense, it is not surprising that the mechanical properties of the TM, which has an intricate, highly organized internal structure, are also frequency-dependent.

The structural complexity of the mammalian TM (24) has been associated with findings that reveal important roles for the TM in the harnessing and distribution of energy and frequency tuning in the mammalian cochlea (14,15,25–27). Despite advances in understanding the physiological

Submitted August 27, 2014, and accepted for publication November 4, 2014.

*Correspondence: a.lukashkin@brighton.ac.uk or i.russell@brighton.ac.uk

G. P. Jones's present address is University College London Ear Institute, 332 Grays Inn Road, London, WC1X 8EE, United Kingdom.

Editor: Charles Wolgemuth.

0006-3495/15/01/0203/8 $2.00

http://dx.doi.org/10.1016/j.bpj.2014.11.1854

importance of the TM, it is not known, as yet, which part of the TM's intricate structure is responsible for its complex, frequency-dependent material properties. The most complex structural component of the TM appears to be the core, which is composed of radial bands of collagen fibers imbedded in and structurally organized by a striated sheet matrix (SSM); a quasi-crystalline array of glycoproteins (28,29). The SSM is composed of a number of different proteins, including α-tectorin (Tecta) (25,30,31), β-tectorin (Tectb) (14,26), otogelin (Otog) (32), otolin (33), and Ceacam16 (34), which have been identified with organizing the longitudinal anisotropy of the TM (9–12,35).

In this article, we describe the outcome of experiments designed to determine the frequency-dependent material properties of TM segments extracted from three groups of mice with disrupted or missing SSM. The groups with missing SSM comprise $Tecta^{Y1870C/+}$, lacking expression of α-tectorin (25); and $Tectb^{-/-}$, lacking expression of β-tectorin (14). In the third group, we have the $Otoa^{EGFP/EGFP}$ mice, which lack the expression of otoancorin (27,36). Although the structure of SSM is largely unaffected, the SSM is missing from the region overlying the OHCs (27). In humans, mutations of $Tecta^{Y1870C/+}$ and $Otoa^{EGFP/EGFP}$ are causes of hereditary deafness (10,37,38). We used a laser interferometer to measure the longitudinal propagation of radial, shearing, traveling-waves along the lengths of TM segments isolated from the basal, high-frequency, turns of the cochleae. The outcomes of these measurements are discussed with respect to known physicochemical properties of the TM and in vivo measurements of the acoustical, mechanical, and electrical responses of the cochlea.

MATERIALS AND METHODS

Preparation of TM samples

Data from the basal cochlear region were collected from $Tecta^{Y1870C/+}$, $Tectb^{-/-}$, and $Otoa^{EGFP/EGFP}$ mice (of between 1 and 6 months of age) on CBA/Ca backgrounds. Mice were euthanized by CO_2 and dissections were performed under a light microscope, in a Petri dish containing artificial endolymph (174 mM KCl, 2.00 mM NaCl, 0.0261 mM $CaCl_2$, 3.00 mM D-glucose, and 5.00 mM HEPES, pH = 7.3). The inner ear was removed from the skull and the cochlea was opened with forceps. The TM was detached from the spiral limbus (if necessary) using a tungsten probe with a tip diameter of <0.1 mm, and cut with a scalpel blade into segments between 350- and 1000-μm long. A segment, cut from the basal one-third of the detached TM, was transferred into the pre-prepared experimental chamber using a glass-tipped pipette and mounted.

Traveling wave excitation and measurements

Experiments were conducted using the method previously described in Jones et al. (19) in a quiet room, on a vibration isolation table, and inside a Faraday cage. The experimental chamber was filled with artificial endolymph so that the prepared TM was submerged to a depth of at least 4 mm. Cell-Tak (BD Biosciences, San Jose, CA) was used to attach a single segment of TM to a vibrating support (~5 × 10 × <1 mm) attached to a stimulation piezo (model No. AE0203D04; ThorLabs, Newton, NJ), and a mechanically isolated stationary support (~10 × 10 × <1 mm) (Fig. 1). The stimulation piezo was mounted rigidly to the microscope slide forming the base of the chamber. A lab-built, self-mixing, homodyne laser-diode interferometer (39) aimed through a viewing window in the front wall was used to record the phase and amplitude of traveling wave at multiple points along the mounted segment of TM.

The beam of the laser interferometer was focused onto the marginal edge of the TM near the vibrating support so that the light entering the chamber was approximately parallel with the end of the vibrating support. Recording commenced from this point, and the laser beam was stepped along the TM (in 10- or 20-μm steps, typically with 3–5 repetitive measurements for each position) until it came within 100 μm of the stationary support or a segment of at least 300 μm had been covered for each TM preparation. Radial sinusoidal stimulation of 2–20 kHz was applied to the TM via the vibrating support in steps of 1 kHz at every longitudinal position. Measurements <2 kHz and >20 kHz were not reliable due to small phase gradients (<1/8 of a cycle) at low frequencies and small amplitude of vibrations, which approached the noise floor of ~0.5–5 nm (measured <300 μm from the piezo), and, hence, resulted in a low signal/noise at high frequencies. Amplitude data were calibrated to control for variable reflectance at each point along the TM using a piezo with known displacement, on which the laser diode was mounted.

Calculation of material properties of the TM

Shear modulus, $G'(\omega)$, and shear viscosity, $\eta(\omega)$ of the TM were calculated using a model of the TM in fluid environment (19). Namely, shear modulus and shear viscosity were calculated from the equation

$$G'(\omega) + i\omega\eta(\omega) = \frac{\omega^2\left(T_{TM}\rho_{TM} + \sqrt{2}\delta\rho_f\right) - i\sqrt{2}\omega^2\rho_f\delta}{k^2(\omega)T_{TM}}, \quad (1)$$

where ω is angular frequency, T_{TM} is thickness of the TM (2×10^{-5} m), ρ_f and ρ_{TM} are the fluid density and the TM density, respectively (both are taken to be 10^3 kg m^{-3}), k is the complex wavenumber, and δ is the boundary layer thickness, which was determined as

$$\delta = \sqrt{\frac{\mu}{\omega\rho_f}}, \quad (2)$$

where μ is the coefficient of viscosity (7×10^{-4} kg m^{-1} s^{-1}). The complex wavenumber can be calculated from the measured wave speed, c, and decay constant, α, as

Mounted TM

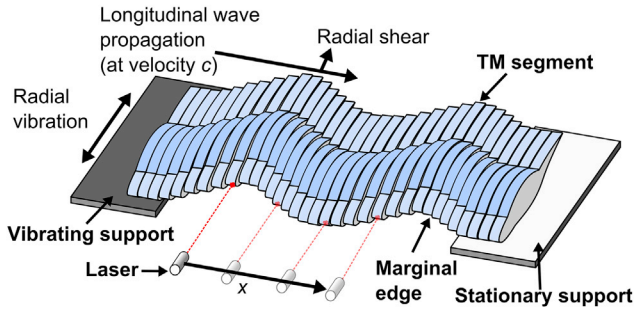

FIGURE 1 Schematic of the inside of the experimental chamber, containing a mounted segment of TM, attached to both supports. Stimulation was delivered by the vibrating support, which was attached to a piezoelectric actuator, and a single laser was stepped along the TM to track amplitude and phase of radially shearing, longitudinally propagating traveling waves at different frequencies. To see this figure in color, go online.

$$k(\omega) = \frac{\omega}{c} - i\alpha. \quad (3)$$

Note that if the viscosity and hence the boundary layer thickness tends to zero, the right-hand side of Eq. 1 just reverts to the complex shear modulus, as

$$k(\omega) = \frac{\omega}{c(\omega)}, \quad (4)$$

where $c(\omega)$ is the frequency-dependent shear wave speed, which is equal to the square-root of the complex shear modulus divided by the TM density, so that

$$c^2(\omega) = \frac{G'(\omega) + i\omega\eta(\omega)}{\rho_{TM}}. \quad (5)$$

RESULTS

Frequency-dependent propagation of longitudinal traveling waves was investigated in segments of TM isolated from the basal (high-frequency) region of cochleae from *Tecta*$^{Y1870C/+}$, *Tectb*$^{-/-}$, and *Otoa*$^{EGFP/EGFP}$ mice, with mutations or deletions of the TM proteins, α-tectorin, β-tectorin, and otoancorin. Measurements were confined to the basal region, because it was in this region that the propagation of longitudinal traveling waves along the TM showed greatest frequency dependency (19). Longitudinally propagating traveling shear waves were excited in the TM by sinusoidal vibration of the piezoelectric actuator (Fig. 1) and the amplitude and phase of the radial displacement due to the traveling wave, as functions of distance from the source of excitation, were measured with a laser diode interferometer (39). These data provided the basis for deriving the dynamic material properties of the TM.

Velocity of the TM traveling waves decreases when SSM is disrupted or missing

The traveling wave velocity was calculated from the progressive phase lag measured as a function of longitudinal distance from the vibrating platform ($x = 0$ μm). In modified TMs from all three groups of mice, the phase lag increased as a function of stimulation frequency (2–20 kHz) (Fig. 2, *A–C*).

The propagation velocity, c, of the traveling waves was calculated at each frequency, ω, as $c = \omega \times x/\Delta\varphi$, where $\Delta\varphi$ is the overall change in phase over the longest measurement distance x for each segment, i.e., average velocity over distance x was calculated. The means and standard error of c at each frequency are shown in Fig. 2 *D* and compared to previously published data from normal, wild-type TMs (19).

Propagation velocity in TM segments taken from mice with disrupted or missing SSM increased as a function of stimulus frequency. The velocity increase with frequency was similar for all three groups, increasing

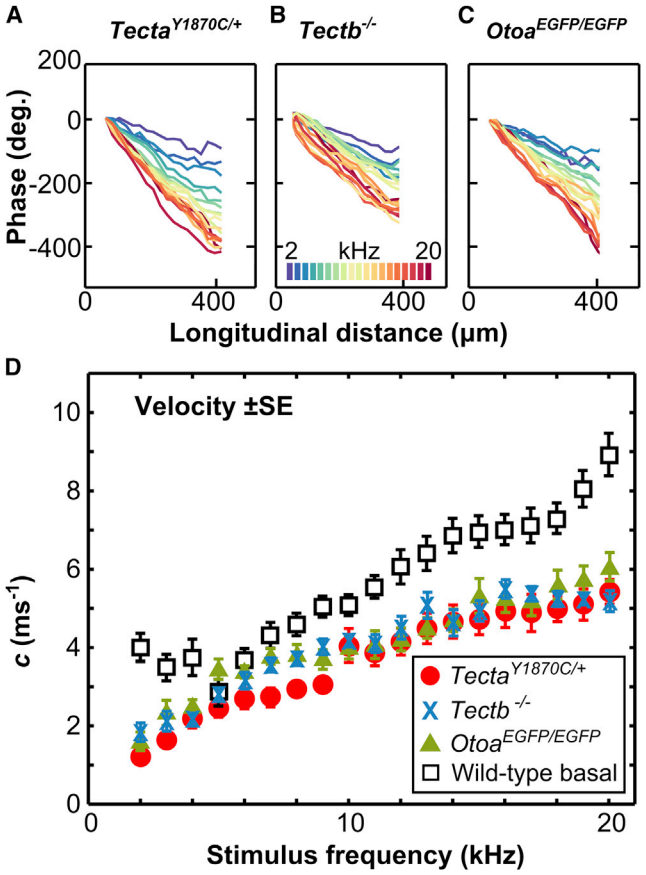

FIGURE 2 Phase data collected from the basal TM segments of *Tecta*$^{Y1870C/+}$, *Tectb*$^{-/-}$, and *Otoa*$^{EGFP/EGFP}$ mice. (*A–C*) Average phase lag as a function of longitudinal distance along the TM segments, for each stimulus frequency (for clarity, error bars are not shown). (*D*) Average wave propagation velocity, calculated from the full longitudinal distance obtained in each experiment (*Tecta*$^{Y1870C/+}$ $n = 12$, *Tectb*$^{-/-}$ $n = 14$, and *Otoa*$^{EGFP/EGFP}$ $n = 12$ mean ± SE), includes wild-type data previously collected from the basal cochlear region for comparison (19).

from ~1.5 m s^{-1} at 2 kHz to 5.5 m s^{-1} at 20 kHz. Apart from the propagation velocity minima at 5 kHz, propagation velocities measured from the wild-type mice (*black squares*; Fig. 2 *D*) are significantly higher than those measured in the groups with modified TM, especially at the highest stimulus frequency used (20 kHz).

Amplitude decay of TM traveling wave increases when SSM is disrupted or missing

The amplitude of the traveling wave also decays with distance along the TM. The decay constant, α, was derived by fitting an exponential decay to the wave amplitude, $Y(x)$ as a function of longitudinal distance x, namely, $Y(x) = Y(0)e^{-\alpha x}$, where $Y(0)$ is the wave amplitude at the stimulation place.

The decay constant tended to decrease with increasing stimulus frequency in TM segments isolated from the wild-type mice (Jones et al. (19); see *squares* in Fig. 3).

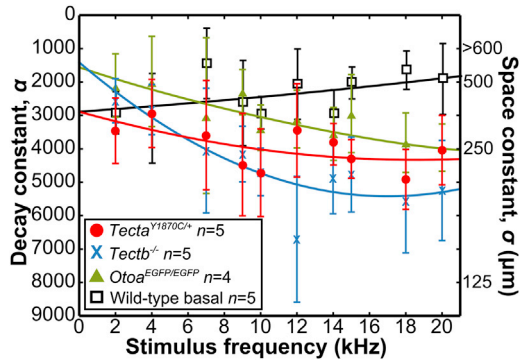

FIGURE 3 Amplitude decay (±SD) and space constants of the traveling wave as a function of frequency for basal TM segments. (*Solid lines*) Polynomial fit to the data points of $Tecta^{Y1870C/+}$ ($\alpha = -2887\text{-}0.158f + 0.00000434f^2$, $r^2 = 0.39$), $Tectb^{-/-}$ ($\alpha = -1372\text{-}0.494f + 0.0000151f^2$, $r^2 = 0.75$), and $Otoa^{EGFP/EGFP}$ ($\alpha = -1550\text{-}0.182f + 0.000000274f^2$, $r^2 = 0.79$) mice. The figure also includes previously collected wild-type data from the basal cochlear region (19).

For all three groups with modified SSM, however, the decay constant increased with increasing frequency over the same stimulus frequency range (Fig. 3). An increase in α corresponds to a decrease in the space constant (σ), which represents the spatial extent of the wave's propagation (Fig. 3).

The mechanical properties of the TM are affected by structural disruption of SSM

The viscoelastic properties, namely the shear storage modulus, $G'(\omega)$, and shear viscosity, $\eta(\omega)$, were calculated at discrete frequencies from the wave propagation velocity, $c(\omega)$, and the decay constant, $\alpha(\omega)$, using Eqs. 1 and 3 (Materials and Methods). These properties had previously been found to be highly dependent on stimulus frequency when measured from TM segments isolated from the basal turn of the wild-type mice (19). The shear viscosity, $\eta(\omega)$, which was shown in the wild-type mice to decrease 8.4-fold with increasing frequency ranging 2–10 kHz (*squares*; Fig. 4 *B*), was found here to be almost independent of frequency in all three groups with disrupted or missing SSM (*circles*, *crosses*, and *triangles*; Fig. 4 *B*).

The shear storage modulus, $G'(\omega)$ measured from TM segments isolated from the basal region of all three groups of mice with modified TMs, increased as a function of stimulus frequency, ranging 2.52–31.2 kPa for $Tecta^{Y1870C/+}$, 4.46–29.7 kPa for $Tectb^{-/-}$, and 4.63–41.2 kPa for $Otoa^{EGFP/EGFP}$, between 2 and 20 kHz (*circles*, *crosses*, and *triangles*; Fig. 4 *A*). These increases are small when compared with those obtained from similar measurements made from wild-type mice, where $G'(\omega)$ increased over the same stimulus frequency range of 6.50–80.1 kPa (*squares*; Fig. 4 *A*). Note that <5 kHz, the frequency dependence (and even the absolute magnitude) of $G'(\omega)$ is similar for the wild-type mice and for the groups of mice with modified TMs.

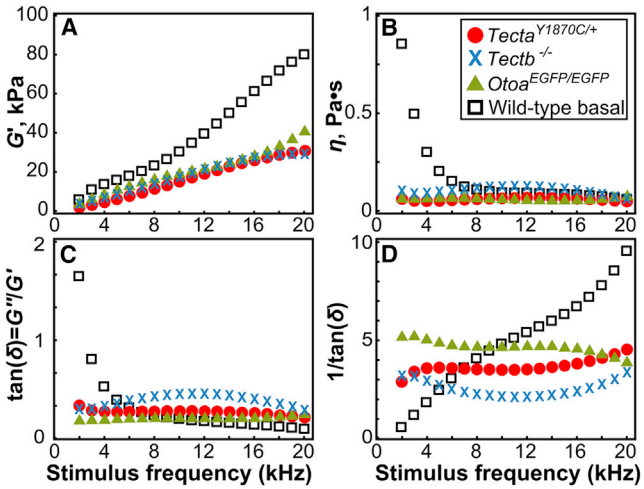

FIGURE 4 Frequency dependence of the dynamic material properties of the TM. Equations 1 and 3 (Materials and Methods) and the experimental data presented in Fig. 2 *C* and Fig. 3 were used for calculations. (*A*) Shear storage modulus, G'. (*B*) Shear viscosity, η. (*C*) Loss tangent, tanδ and (*D*) reciprocal of the loss tangent, 1/tanδ, which is proportional to the quality factor Q. TM thickness, T_{TM}, was taken as 20 μm for the basal segments. Includes data from wild-type mice previously collected from the basal cochlear region for comparison (19).

It is worth noting that if the effect of the external fluid is ignored, then by setting the boundary layer thickness to zero in the calculation of the complex modulus in Eq. 1, the apparent shear modulus is slightly lower than that calculated here. However, the apparent shear viscosity is significantly increased, because the damping physically due to the fluid is then accounted for in that of the TM.

Energy transmission and dissipation is modified in TMs with disrupted SSM

The loss tangent tanδ, $= G''/G'$, where G'' is the loss modulus (G'' is calculated as $G'' = \omega\eta(\omega)$ using data for $\eta(\omega)$ in Fig. 4 *B*), defines the ratio of energy dissipated to energy stored per volume unit of TM (19) and characterizes the effectiveness of longitudinal energy transmission during shear deformations of the TM (Fig. 4 *C*). The value tanδ calculated for the TM segments isolated from the basal regions of the three groups with modified TM (*circles*, *crosses*, and *triangles*; Fig. 4 *C*) behaved differently as functions of stimulus frequency compared to that of basal turn TM segments of wild-type mice (*squares*; Fig. 4 *C*).

For stimulus frequencies <5 kHz, tanδ calculated for TM segments isolated from the groups with disrupted or missing SSM was significantly lower than that of tanδ calculated for TM segments of the wild-type mice. In other words, at these low frequencies, the relative dissipation of energy is lower in the modified TMs than in the wild-type mice. At 20 kHz, however, tanδ for the wild-type mice is approximately one-half of that for any group with disrupted or missing SSM and, hence, the TM in the wild-type mice is more

efficient at transmitting energy at stimulus frequencies approaching the frequency range of the basal turn of the mouse cochlea.

The reciprocal of the loss tangent is proportional to the quality factor, $(Q \propto 1/\tan(\delta) = G'/G'')$, which describes the resonant material properties of the TM (Fig. 4 *D*). In the segments from all groups with modified TMs (*circles*, *crosses*, and *triangles*; Fig. 4 *D*), Q is relatively independent of frequency, while in the TM segments isolated from the wild-type mice (*squares*; Fig. 4 *D*), there is a very clear rise in the value of Q with increasing frequency. In all three groups with disrupted or missing SSM, there is less variation in Q with frequency across the 2–20 kHz range than in segments isolated from the wild-type cochleae.

DISCUSSION

In vitro traveling wave propagation is disrupted in all three mutant groups with compromised striated sheet matrix

The velocities of traveling waves measured in segments of TM isolated from the cochleae of $Tecta^{Y1870C/+}$, $Tectb^{-/-}$, and $Otoa^{EGFP/EGFP}$ mice were all similarly and significantly reduced by comparison with traveling wave velocities measured in segments of TM isolated from the same region of the cochleae of wild-type mice (Fig. 2 *D*). Reductions in the wave velocity were accompanied by an increase in the decay constant for the majority of the measured frequency range (Fig. 3) and are manifested in traveling waves (Fig. 5), which have shorter wavelengths with more rapid decay than those from wild-type TMs. We attribute these differences largely to changes in frequency-dependent stiffness than to shear viscosity. This is because, at least for the frequencies illustrated in Fig. 5 (>8 kHz), the shear viscosity of TMs isolated from wild-type mice and those with genetically modified protein composition are similar (Fig. 4 *B*). The only major structural component of the TM, which, as far as we are aware, is altered in common in the genetically modified mice used in this study, is the SSM. It is completely absent in the $Tectb^{-/-}$ mouse (14) and partially lost in the $Tecta^{Y1870C/+}$mouse (25), including a marginal region where, in the TM of $Otoa^{EGFP/EGFP}$ mice, it is specifically absent.

The marginal region is a zone 20-μm wide (~20% width of the TM), which runs along the lateral edge that overlies the OHCs (27). It is the stiffest part of the TM and, in the basal turn of the cochlea, is the only region of the TM that becomes increasingly stiffer with increasing frequency place on the BM (8,40). Gueta et al. (40) presumed that the place-dependent stiffness gradient of this zone was to facilitate energy transfer with the OHC hair bundles, whose stiffness also increases with increasing distance from the apex of the cochlea (41,42). It would appear, according to the findings reported here, that any loss of SSM, especially in the hair-bundle attachment zone of the TM, is associated with a loss of the frequency-dependent stiffness of the material properties of the TM.

Findings related to the frequency-dependency of mechanical properties of the TM reported here are considered new

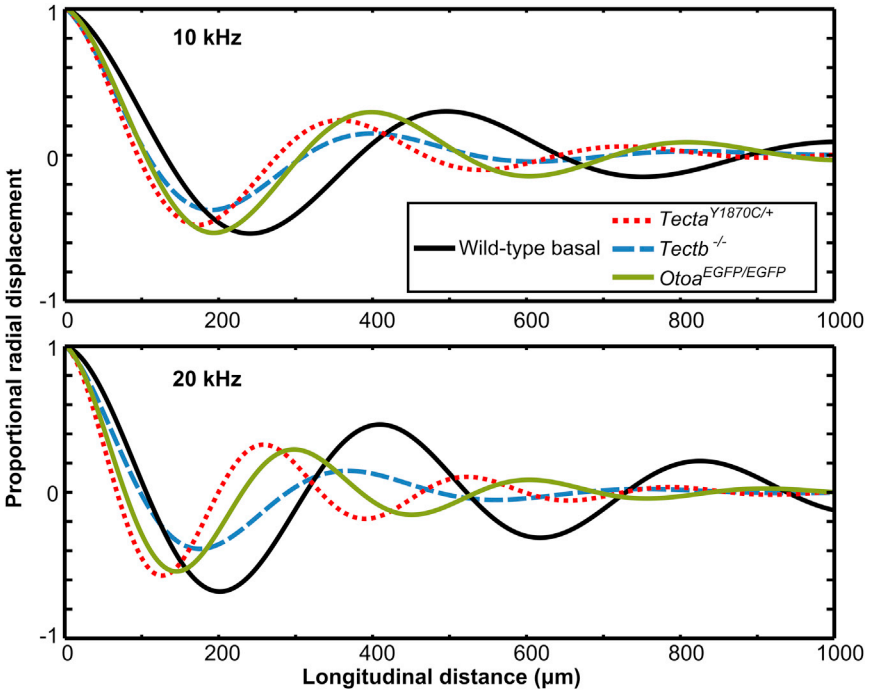

FIGURE 5 Recreated instantaneous traveling waveforms calculated from the accumulated phase lag and decay constant at 10 and 20 kHz, respectively, for all groups of mice. To see this figure in color, go online.

and novel, although the measurements of the mechanical properties of the TM upon which they are based are similar to those reported previously for individual frequencies, using similar methods, from mice with genetic modification of the TM (26,43).

Note that the complex shear modulus calculated here is of the TM alone. When the TM is integrated into the organ of Corti, its dynamics will be influenced by the stiffness of the OHC stereocilia, which will tend to increase the shear wave speed; and the viscosity of the fluid in the subtectorial space, which will tend to increase the damping. Assuming the geometry of the subtectorial space is similar in the wild-type and genetically modified mice, these effects, however, will be the same in all groups of mice and the differences seen here for the TM alone will also be reflected in the in situ TM dynamics.

Disruption or absence of the striated sheet matrix largely abolishes frequency dependence of the TM mechanical properties

The organization of the TM is complex, with radial collagen fibers and interconnecting noncollagenous glycoproteins forming the quasi-crystalline striated sheet matrix (28,29). This complexity has led to the suggestion that the array structure and different packing density of collagen fibers form a basis for longitudinal, radial, and transversal gradients of the TM's mechanical properties (8–12). We further suggest that the striated sheet matrix provides a specific structural basis for the frequency dependency of the material properties of the TM (19).

Insight into the physical basis for the frequency dependence of the mechanical properties of the TM may be deduced from what is currently understood about the physical chemistry of the TM. In a conceptual model by Masaki et al. (44), the TM is considered as a porous matrix, consisting of solid and fluid phases with the fluid phase moving through pores of a limited size. At asymptotically low frequencies, the elasticity of the solid phase, namely the elasticity of interconnected collagen fibers, is the dominating component of the TM stiffness. With increasing stimulation frequency, the viscosity of fluid moving through the relatively small pores of the TM matrix would be expected to contribute significantly toward the TM's mechanical properties, thereby creating a possible basis for their frequency dependence.

Indeed, changes in the viscosity of the TM's fluid phase are associated with prominent changes in TM electrokinetic response (45), indicating the importance of fluid movement within the TM during its deformation. If in TMs with missing or genetically modified proteins, the porous structure is altered, as found by Masaki et al. (43) for TM isolated from $Tecta^{Y1870C/+}$ mice, the contribution from the viscosity of the fluid phase might be reduced with a consequent reduction or abolition of the frequency dependency of the TM mechanical properties. Such changes in the shear viscosity of the TM has been shown to modify propagation of waves in the TM with important consequences for cochlear tuning in $Tecta^{Y1870C/+}$ mice (46).

Another possible basis for the frequency-dependent mechanical properties of the TM is change in the local density of fixed charges within the TM during its deformation. It has been demonstrated that the TM contains high concentration of fixed charges associated with ionized sulfate (SO_3^-) and carboxyl (COO^-) groups of glycoproteins (7,47) and that electrostatic interaction between them contributes significantly to the compressional stiffness of the TM (45). Furthermore, neutralization of the fixed charges at low pH causes a two-to-threefold reduction in the TM shear impedance (48). Thus, shear deformation of the TM should lead to changes in the local density of the fixed charges and consequent redistribution of mobile ions and fluid phase within the TM according to the principles of electrodiffusive, osmotic, and mechanical equilibrium, and bulk electroneutrality (47).

The time taken to reach the equilibrium is limited by the poroelastic relaxation time, which is of the order of tens of minutes (7,44,49) and can affect the mechanical responses of the TM at acoustic frequencies (45). If electrostatic interaction between the fixed charges contributes to the frequency dependence of the TM mechanical properties, then the decreased frequency-dependent stiffness we have observed in TMs from $Tecta^{Y1870C/+}$, $Tectb^{-/-}$, and $Otoa^{EGFP/EGFP}$ mice could be due to a consequent reduction in density of the associated fixed charges in the TM, as has indeed been reported for $Tecta^{Y1870C/+}$ mice (43). A likely source of the fixed charges, which is disrupted in all three mouse mutants used in this study, is the SSM which, because of its composition and structural organization, is likely to have a dense, highly organized distribution of fixed charges.

Because both porosity and fixed charges within the TM determine its mechanical properties (44,45,48), it is likely that combinations of both these factors determine specific frequency dependence of the TM dynamic material properties (19). It should be remembered that enhanced tuning of the TM (14) comes at a price. Fewer OHCs are engaged to amplify a single frequency place on the BM, with subsequent loss, albeit relatively small, of sensitivity (14,18). It would appear that sensitivity of the cochlea, rather than enhanced frequency tuning of the TM, has greater survival value.

Forward energy transmission is not affected in mice with missing or disrupted striated sheet matrix

It has been hypothesized that a reduction of stiffness of the basal TM at low frequencies leads to functional decoupling of the TM from the cochlear partition, which minimizes

energy loss and facilitates energy transmission along the cochlea to the cochlear apex (19). At the same time, stiffening of the basal TM at high frequencies (19) maximizes cochlear amplifier gain through better elastic coupling along the TM (14,16). The effectiveness of energy transmission (loss tangent, tanδ, Fig. 4 *C*), which is relatively large at frequencies >8 kHz for TM segments from mice with deleted or altered TM proteins compared to those of TM segments from wild-type mice, is expected not to lead to higher energy losses from the modified TMs in vivo. This is because the TM in the basal region of the cochlea would not experience significant radial shear during the propagation of low-frequency BM traveling waves.

The waves peak at their characteristic frequency place, which is closer to the cochlear apex, and do not show significant phase change in the basal region (6). In vivo, the TM in the basal region of the cochlea experiences significant shear at frequencies that are close to the characteristic frequencies of that region (~35–60 kHz for the isolated TM segments used in our experiments). Hence, higher energy losses from TMs of $Tecta^{Y1870C/+}$, $Tectb^{-/-}$, and $Otoa^{EGFP/EGFP}$ mice, compared with wild-type mice, are expected only for frequencies near the characteristic frequencies of the basal turn, but propagation of energy to the characteristic place should not be affected.

Physiological consequences of changes in mechanical properties of mutant TMs

The physiological phenotypes expressed by $Tecta^{Y1870C/+}$, $Tectb^{-/-}$, and $Otoa^{EGFP/EGFP}$ mice reveal an important similarity and differences. Total loss of SSM, as in $Tectb^{-/-}$ mice, is associated with loss of elastic coupling along the TM in vivo (14,16) and, therefore the presence of β-tectorin is necessary for maintaining the SSM and velocity and spatial extent of traveling waves in vitro (15,19,26). In $Tectb^{-/-}$ and $Tecta^{Y1870C/+}$ mice, where SMM loss is not restricted to the hair-bundle attachment zone in the TM, gain and sensitivity of BM responses in the 50–60 kHz region of the cochlea are reduced by ~10 dB SPL compared with measurements from wild-type littermates (14,25) and $Otoa^{EGFP/EGFP}$ mice (27).

These measurements, which reveal that the sensitivity of tone-evoked BM vibrations is changed only slightly or imperceptibly, provide evidence that forward energy transmission is not affected in the basal turn of the cochlea in these mutants. The loss of sensitivity of BM motion measured in $Tectb^{-/-}$ and $Tecta^{Y1870C/+}$ mice, where there is total or partial loss of SSM distributed throughout the TM, may be a consequence of imperfect impedance matching and hence transfer of energy, between the stiffness of the OHC hair bundles and that of the TM; or may be a consequence of changes in elastic (14,15,19) and viscous coupling (46) along the TM with corresponding changes in the spread of excitation within the cochlea and reduction in cochlear gain (14,16). $Tecta^{Y1870C/+}$, $Tectb^{-/-}$, and $Otoa^{EGFP/EGFP}$ mice do, however, share a common physiological phenotype.

Changes in the mechanical properties of the TM of all three mutants effect interaction between tones in the cochlea and the backward transmission of energy from the cochlea, because of this interaction, as revealed in measurements of DPOAE isothreshold responses. DPOAE thresholds are increased, in comparison with those from wild-type littermates, by ~20 dB across the stimulus frequency range (2–60 kHz) in $Tecta^{Y1870C/+}$ and $Otoa^{EGFP/EGFP}$ mice (25,27).

In addition, DPOAE generation in $Tectb^{-/-}$ mice appears to have a velocity dependency, possibly associated with loss of elastic coupling along the TM. Thus, for the products of interaction between tones in the cochlea, the TM appears to act as the conduit for energy transfer along the organ of Corti, a process that is severely attenuated in the TMs of mice where the SSM is missing, at least from the hair-bundle attachment zone of the TM. Regardless of what other structures have been implicated in the transmission of emission energy along the cochlea (50), frequency-dependent properties of the TM are essential for the generation and transmission of DPOAEs along the BM. This finding has consequences in the clinic for subjects with congenital hearing loss due to absence or modification of TM proteins, where there may be a mismatch between hearing assessed through measurement of DPOAEs and more direct measures of cochlear responses.

ACKNOWLEDGMENTS

We thank James Hartley for the design and construction of electronic equipment and Guy Richardson for comments on an early version of the article and for supplying the mice used in this study.

This work is supported by a grant from the Medical Research Council. G.P.J. was supported by a Biotechnology and Biological Sciences Research Council studentship.

REFERENCES

1. Russell, I. J. 2008. Cochlear receptor potentials. *In* The Senses: A Comprehensive Reference. A. I. Basbaum, A. Kaneko, G. M. Shepherd, G. Westheimer, T. D. Albright, R. H. Masland, P. Dallos, D. Oertel, S. Firestein, G. K. Beauchamp, M. C. Bushnell, J. H. Kaas, and E. Gardner, editors. Academic Press, New York, pp. 319–358.
2. Békésy, G. v. 1960. Experiments in Hearing. McGraw-Hill, New York.
3. Kimura, R. S. 1966. Hairs of the cochlear sensory cells and their attachment to the tectorial membrane. *Acta Otolaryngol.* 61:55–72.
4. Davis, H. 1983. An active process in cochlear mechanics. *Hear. Res.* 9:79–90.
5. Lukashkin, A. N., M. N. Walling, and I. J. Russell. 2007. Power amplification in the mammalian cochlea. *Curr. Biol.* 17:1340–1344.
6. Robles, L., and M. A. Ruggero. 2001. Mechanics of the mammalian cochlea. *Physiol. Rev.* 81:1305–1352.
7. Freeman, D. M., C. C. Abnet, …, T. F. Weiss. 2003. Dynamic material properties of the tectorial membrane: a summary. *Hear. Res.* 180:1–10.

8. Gueta, R., D. Barlam, …, I. Rousso. 2006. Measurement of the mechanical properties of isolated tectorial membrane using atomic force microscopy. *Proc. Natl. Acad. Sci. USA.* 103:14790–14795.
9. Richter, C.-P., G. Emadi, …, P. Dallos. 2007. Tectorial membrane stiffness gradients. *Biophys. J.* 93:2265–2276.
10. Richardson, G. P., A. N. Lukashkin, and I. J. Russell. 2008. The tectorial membrane: one slice of a complex cochlear sandwich. *Curr. Opin. Otolaryngol. Head Neck Surg.* 16:458–464.
11. Gavara, N., and R. S. Chadwick. 2009. Collagen-based mechanical anisotropy of the tectorial membrane: implications for inter-row coupling of outer hair cell bundles. *PLoS ONE.* 4:e4877.
12. Teudt, I. U., and C. P. Richter. 2014. Basilar membrane and tectorial membrane stiffness in the CBA/CaJ mouse. *J. Assoc. Res. Otolaryngol.* 15:675–694.
13. Hubbard, A. 1993. A traveling-wave amplifier model of the cochlea. *Science.* 259:68–71.
14. Russell, I. J., P. K. Legan, …, G. P. Richardson. 2007. Sharpened cochlear tuning in a mouse with a genetically modified tectorial membrane. *Nat. Neurosci.* 10:215–223.
15. Ghaffari, R., A. J. Aranyosi, and D. M. Freeman. 2007. Longitudinally propagating traveling waves of the mammalian tectorial membrane. *Proc. Natl. Acad. Sci. USA.* 104:16510–16515.
16. Meaud, J., and K. Grosh. 2010. The effect of tectorial membrane and basilar membrane longitudinal coupling in cochlear mechanics. *J. Acoust. Soc. Am.* 127:1411–1421.
17. Gummer, A. W., W. Hemmert, and H. P. Zenner. 1996. Resonant tectorial membrane motion in the inner ear: its crucial role in frequency tuning. *Proc. Natl. Acad. Sci. USA.* 93:8727–8732.
18. Lukashkin, A. N., G. P. Richardson, and I. J. Russell. 2010. Multiple roles for the tectorial membrane in the active cochlea. *Hear. Res.* 266:26–35.
19. Jones, G. P., V. A. Lukashkina, …, A. N. Lukashkin. 2013. Frequency-dependent properties of the tectorial membrane facilitate energy transmission and amplification in the cochlea. *Biophys. J.* 104:1357–1366.
20. Yamada, S., D. Wirtz, and S. C. Kuo. 2000. Mechanics of living cells measured by laser tracking microrheology. *Biophys. J.* 78:1736–1747.
21. Deng, L., X. Trepat, …, J. J. Fredberg. 2006. Fast and slow dynamics of the cytoskeleton. *Nat. Mater.* 5:636–640.
22. Stamenović, D., N. Rosenblatt, …, D. E. Ingber. 2007. Rheological behavior of living cells is timescale-dependent. *Biophys. J.* 93:L39–L41.
23. Roy, S., W. E. Brownell, and A. A. Spector. 2012. Modeling electrically active viscoelastic membranes. *PLoS ONE.* 7:e37667.
24. Goodyear, R. J., and G. P. Richardson. 2002. Extracellular matrices associated with the apical surfaces of sensory epithelia in the inner ear: molecular and structural diversity. *J. Neurobiol.* 53:212–227.
25. Legan, P. K., V. A. Lukashkina, …, G. P. Richardson. 2005. A deafness mutation isolates a second role for the tectorial membrane in hearing. *Nat. Neurosci.* 8:1035–1042.
26. Ghaffari, R., A. J. Aranyosi, …, D. M. Freeman. 2010. Tectorial membrane traveling waves underlie abnormal hearing in Tectb mutant mice. *Nat. Commun.* 1:96.
27. Lukashkin, A. N., P. K. Legan, …, G. P. Richardson. 2012. A mouse model for human deafness DFNB22 reveals that hearing impairment is due to a loss of inner hair cell stimulation. *Proc. Natl. Acad. Sci. USA.* 109:19351–19356.
28. Hasko, J. A., and G. P. Richardson. 1988. The ultrastructural organization and properties of the mouse tectorial membrane matrix. *Hear. Res.* 35:21–38.
29. Tsuprun, V., and P. Santi. 1997. Ultrastructural organization of proteoglycans and fibrillar matrix of the tectorial membrane. *Hear. Res.* 110:107–118.
30. Legan, P. K., V. A. Lukashkina, …, G. P. Richardson. 2000. A targeted deletion in α-tectorin reveals that the tectorial membrane is required for the gain and timing of cochlear feedback. *Neuron.* 28:273–285.
31. Xia, A., S. S. Gao, …, J. S. Oghalai. 2010. Deficient forward transduction and enhanced reverse transduction in the α-tectorin C1509G human hearing loss mutation. *Dis. Model. Mech.* 3:209–223.
32. Simmler, M.-C., M. Cohen-Salmon, …, J.-J. Panthier. 2000. Targeted disruption of Otog results in deafness and severe imbalance. *Nat. Genet.* 24:139–143.
33. Deans, M. R., J. M. Peterson, and G. W. Wong. 2010. Mammalian Otolin: a multimeric glycoprotein specific to the inner ear that interacts with otoconial matrix protein Otoconin-90 and Cerebellin-1. *PLoS ONE.* 5:e12765.
34. Zheng, J., K. K. Miller, …, P. Dallos. 2011. Carcinoembryonic antigen-related cell adhesion molecule 16 interacts with α-tectorin and is mutated in autosomal dominant hearing loss (DFNA4). *Proc. Natl. Acad. Sci. USA.* 108:4218–4223.
35. Freeman, D. M., K. Masaki, …, T. F. Weiss. 2003. Static material properties of the tectorial membrane: a summary. *Hear. Res.* 180:11–27.
36. Zwaenepoel, I., M. Mustapha, …, C. Petit. 2002. Otoancorin, an inner ear protein restricted to the interface between the apical surface of sensory epithelia and their overlying acellular gels, is defective in autosomal recessive deafness DFNB22. *Proc. Natl. Acad. Sci. USA.* 99:6240–6245.
37. Richardson, G. P., J. B. de Monvel, and C. Petit. 2011. How the genetics of deafness illuminates auditory physiology. *Annu. Rev. Physiol.* 73:311–334.
38. Avraham, K. B., and M. Kanaan. 2012. Genomic advances for gene discovery in hereditary hearing loss. *J. Basic Clin. Physiol. Pharmacol.* 23:93–97.
39. Lukashkin, A. N., M. E. Bashtanov, and I. J. Russell. 2005. A self-mixing laser-diode interferometer for measuring basilar membrane vibrations without opening the cochlea. *J. Neurosci. Methods.* 148:122–129.
40. Gueta, R., E. Tal, …, I. Rousso. 2007. The 3D structure of the tectorial membrane determined by second-harmonic imaging microscopy. *J. Struct. Biol.* 159:103–110.
41. Russell, I. J., M. Kössl, and G. P. Richardson. 1992. Nonlinear mechanical responses of mouse cochlear hair bundles. *Proc. Biol. Sci.* 250:217–227.
42. Géléoc, G. S. G., G. W. T. Lennan, …, C. J. Kros. 1997. A quantitative comparison of mechanoelectrical transduction in vestibular and auditory hair cells of neonatal mice. *Proc. Biol. Sci.* 264:611–621.
43. Masaki, K., R. Ghaffari, …, A. J. Aranyosi. 2010. Tectorial membrane material properties in $Tecta^{Y1870C/+}$ heterozygous mice. *Biophys. J.* 99:3274–3281.
44. Masaki, K., T. F. Weiss, and D. M. Freeman. 2006. Poroelastic bulk properties of the tectorial membrane measured with osmotic stress. *Biophys. J.* 91:2356–2370.
45. Ghaffari, R., S. L. Page, …, D. M. Freeman. 2013. Electrokinetic properties of the mammalian tectorial membrane. *Proc. Natl. Acad. Sci. USA.* 110:4279–4284.
46. Sellon, J. B., R. Ghaffari, …, D. M. Freeman. 2014. Porosity controls spread of excitation in tectorial membrane traveling waves. *Biophys. J.* 106:1406–1413.
47. Weiss, T. F., and D. M. Freeman. 1997. Equilibrium behavior of an isotropic polyelectrolyte gel model of the tectorial membrane: the role of fixed charges. *Aud. Neurosci.* 3:351–361.
48. Farrahi, S., R. Ghaffari, and D. M. Freeman. 2011. Lowered pH alters decay but not speed of tectorial membrane waves. *In* What Fire is in Mine Ears: Progress in Auditory Biomechanics. Proceedings of the 11th International Mechanics of Hearing Workshop, Williamstown, MA. AIP Conference Proceedings, Vol. 1403. American Institute of Physics. 403. http://dx.doi.org/10.1063/1.3658119.
49. Freeman, D. M., S. Hattangadi, and T. F. Weiss. 1997. Osmotic responses of the isolated mouse tectorial membrane to changes in pH. *Aud. Neurosci.* 3:363–375.
50. Fisher, J. A., F. Nin, …, A. J. Hudspeth. 2012. The spatial pattern of cochlear amplification. *Neuron.* 76:989–997.